Abstract: Nd^{3+}-doped $LaBO_2MoO_4$ with non-centrosymmetric monoclinic structure is presented as a new laser crystal. By Xe-flashlamp pumping at 300 K its pulsed stimulated emission (SE) at two wavelengths of the $^4F_{3/2} \rightarrow {}^4I_{11/2}$ generation channel was excited. A tentative identification of the observed SE transitions and measurements of some spectroscopic characteristics are given. The occurrence of a structural phase transition with a large temperature hysteresis was proved by means of thermal analysis. Despite of this, large crystals of $LaBO_2MoO_4$:Nd^{3+} were grown by the top-seeding method. Based on its SE- and $(\chi^{(2)} + \chi^{(3)})$-active properties we classify this crystal as a promising material for self-frequency doubling and self-Raman lasers.

Sample of $(La_{1-x}Nd_x)BO_2MoO_4$ prepared from a crystal grown from the melt

Monoclinic $LaBO_2MoO_4$:Nd^{3+} – a new SE- and $(\chi^{(2)} + \chi^{(3)})$-active crystal for multifunctional lasers

P. Becker, [1,*] *B. van der Wolf,* [1] *L. Bohatý,* [1] *J. Dong,* [2] *and A.A. Kaminskii* [3,*]

[1] Institute of Crystallography, University of Cologne, 50674 Cologne, Germany
[2] Department of Physics, School of Engineering and Physical Sciences, Heriot-Watt University, EH14 4AS Edinburgh, UK
[3] Institute of Crystallography, Russian Academy of Sciences, Moscow 119333, Russia

Received: 23 May 2008, Accepted: 26 May 2008
Published online: 10 June 2008

Key words: Raman laser shifter; non-centrosymmetric crystal; SHG phase matching; $LaBO_2MoO_4$; Nd^{3+} ion luminescence; stimulated emission

PACS: 42.55.Rz, 42.70.Hj, 42.70.Mp, 78.45.+h

1. Introduction

Among the numerous known insulating Nd^{3+}-ion doped laser crystals oxide borates possess a wide range of attractive properties [1]. Most of them are non-centrosymmetric and allow to realize different self-multifunctional laser phenomena by combining their pulsed or CW stimulated emission (SE) of the lasant activator ions with the quadratic ($\chi^{(2)}$) and cubic ($\chi^{(3)}$) nonlinearities of the host crystal (see Table 1). It is appropriate to note here that the first self-frequency doubling (self-FD) effect in a borate crystal doped with Nd^{3+} was observed in β-$Nd_{0.2}Y_{0.8}Al_3(BO_3)_4$ [2] and the first self-stimulated Raman lasing (self-SRS) was excited in crystals of trigonal β-$LaBGeO_5$:Nd^{3+}, for which also the first many-step cascaded nonlinear $\chi^{(2)} \leftrightarrow \chi^{(3)}$ lasing was recorded [3].

Despite the attractive optical properties of borate crystals their widespread use as optical materials is limited due to the difficulties that frequently occur with borate crystal growth. The growth of high quality large single crystals of borates usually suffers from problems that originate

* Corresponding author: e-mail: petra.becker@uni-koeln.de, kaminalex@mail.ru

Crystal	Space group	Non-linearity	Nd^{3+} laser channel	Nonlinear-laser manifestation	Method of crystal growth
$Ca_4YO(BO_3)_3$	$C_s^3 - Cm$	$\chi^{(2)} + \chi^{(3)}$	$^4F_{3/2} \rightarrow {}^4I_{11/2}$ $^4F_{3/2} \rightarrow {}^4I_{13/2}$	self-FD (SE) [a] self-FD (SE)	Czochralski
$Ca_4GdO(BO_3)_3$	$C_s^3 - Cm$	$\chi^{(2)} + \chi^{(3)}$	$^4F_{3/2} \rightarrow {}^4I_{9/2}$ $^4F_{3/2} \rightarrow {}^4I_{11/2}$ $^4F_{3/2} \rightarrow {}^4I_{13/2}$	self-FD (SE) self-FD (SE) self-FD (SE)	Czochralski
LaB_3O_6	$C_{2h}^6 - C2/c$	$\chi^{(3)}$	$^4F_{3/2} \rightarrow {}^4I_{11/2}$		Czochralski
$LaBO_2MoO_4$	$C_2^2 - P2_1$	$\chi^{(2)} + \chi^{(3)}$	$^4F_{3/2} \rightarrow {}^4I_{11/2}$	self-SFM (SRS) [b]	TSSG
β-$LaBGeO_5$	$C_3^2 - P3_1$	$\chi^{(2)} + \chi^{(3)}$	$^4F_{3/2} \rightarrow {}^4I_{11/2}$ $^4F_{3/2} \rightarrow {}^4I_{13/2}$	self-FD (SE) self-SRS (SE) [c] self-DFG [d] self-FD (SE)	Czochralski
$La_2CaB_{10}O_{19}$	$C_2^3 - C2$	$\chi^{(2)} + \chi^{(3)}$	$^4F_{3/2} \rightarrow {}^4I_{11/2}$ $^4F_{3/2} \rightarrow {}^4I_{13/2}$	self-FD (SE) self-FD (SE)	flux
β-$LaSc_3(BO_3)_4$	$D_3^7 - R32$	$\chi^{(2)} + \chi^{(3)}$	$^4F_{3/2} \rightarrow {}^4I_{11/2}$ $^4F_{3/2} \rightarrow {}^4I_{13/2}$	self-FD (SE)	flux
β-$YAl_3(BO_3)_4$ [e]	$D_3^7 - R32$	$\chi^{(2)} + \chi^{(3)}$	$^4F_{3/2} \rightarrow {}^4I_{9/2}$ $^4F_{3/2} \rightarrow {}^4I_{11/2}$ $^4F_{3/2} \rightarrow {}^4I_{13/2}$	self-FD (SE) self-FD (SE) self-SFM (SE) [f] self-FD (SE) self-SFM (SE)	flux
β-$CeSc_3(BO_3)_4$	$D_3^7 - R32$	$\chi^{(2)} + \chi^{(3)}$	$^4F_{3/2} \rightarrow {}^4I_{11/2}$	self-FD (SE)	flux
α-$NdAl_3(BO_3)_4$	$C_{2h}^6 - C2/c$	$\chi^{(3)}$	$^4F_{3/2} \rightarrow {}^4I_{11/2}$		flux
β-$Nd_{0.2}Y_{0.8}Al_3(BO_3)_4$	$D_3^7 - R32$	$\chi^{(2)} + \chi^{(3)}$	$^4F_{3/2} \rightarrow {}^4I_{11/2}$	self-FD (SE)	flux
β-$NdAl_3(BO_3)_4$	$D_3^7 - R32$	$\chi^{(2)} + \chi^{(3)}$	$^4F_{3/2} \rightarrow {}^4I_{11/2}$		flux
β-$NdSc_3(BO_3)_4$	$D_3^7 - R32$	$\chi^{(2)} + \chi^{(3)}$	$^4F_{3/2} \rightarrow {}^4I_{11/2}$ $^4F_{3/2} \rightarrow {}^4I_{13/2}$		flux
β-$GdAl_3(BO_3)_4$	$D_3^7 - R32$	$\chi^{(2)} + \chi^{(3)}$	$^4F_{3/2} \rightarrow {}^4I_{11/2}$ $^4F_{3/2} \rightarrow {}^4I_{13/2}$	self-FD (SE) self-SFM (SE) self-FT (SFM-SE) [g]	flux

[a] Self-FD (SE): self-frequency doubling, i.e., cascaded SHG from arising SE in Nd^{3+}-ion doped crystals with non-laser and laser pumping.
[b] Self-SFM (SRS): self-sum frequency mixing, i.e., cascaded summing parametric generation (up-conversion process) involving the frequency of the pumping and arising Stokes lasing components.
[c] Self-SRS (SE): self-stimulated Raman scattering, i.e., cascaded laser Raman Stokes and anti-Stokes generation by the action of arising SE in Nd^{3+}-ion doped crystals with external laser radiation.
[d] Self-DFG: self-difference frequency generation, i.e., of the pumping (in the visible)and Stokes lasing by the arising one-micron SE of Nd^{3+} ions [3].
[e] Crystals of the compound β-$Nd_{0.034}Y_{0.766}Gd_{0.2}Al_3(BO_3)_4$ with SE at wavelengths of two laser channels $^4F_{3/2} \rightarrow {}^4I_{11/2}$ and $^4F_{3/2} \rightarrow {}^4I_{13/2}$ of Nd^{3+} ions are also known [10], see also [11].
[f] Self-SFM(SE): self-sum-frequency mixing, i.e., cascaded summing parametric generation (up-conversion process) involving the frequency of the pumping and arising SE of Nd^{3+} lasants.
[g] Self-FT (SFM-SE) is the self-frequency-tripling, i.e., cascaded summing parametric lasing involving the frequency of the SE and its SHG of Nd^{3+} lasants [12].

Table 1 Selected nonlinear-laser properties of known borate crystals with Nd^{3+}

e.g. in frequently occurring high melt viscosity, difficulties in melt homogenization, incongruent evaporation of melt constituents, melt inclusions or bubbles in the crystals, structural phase transitions, etc. Therefore, the mastering of growth of large single crystals of optical quality was the prerequisite for borate materials such as β-BaB_2O_4, LiB_3O_5, $Li_2B_4O_7$, or BiB_3O_6 to enter the field of nonlinear optical applications.

In continuation of our investigations of nonlinear-laser borates (undoped BiB_3O_6 [4], $LiGeBO_4$ [5], $K_3Nb_3O_6(BO_3)_2$ [6], $Li_2B_4O_7$ [7], PbB_4O_7 [8]), recently we reported a new nonlinear optical crystal, lanthanum borate molybdate, $LaBO_2MoO_4$ [9], which turned out to be an effective material for many-phonon generation via stimulated Raman scattering (SRS), producing a Stokes and anti-Stokes lasing comb in the visible and near IR wavelength region. In addition to this, second harmonic generation (SHG) and cascaded $\chi^{(3)} \leftrightarrow \chi^{(2)}$ processes were detected. Furthermore, crystals of $LaBO_2MoO_4$ were doped with Nd^{3+} ions, and preliminary results of a spectroscopic investigation indicate that $LaBO_2MoO_4$:Nd^{3+} could be suitable as a gain material for solid state lasers [9]. In this letter we present our results of crystal growth of Nd^{3+}-doped $LaBO_2MoO_4$ and report on a study of pulsed SE in this crystal.

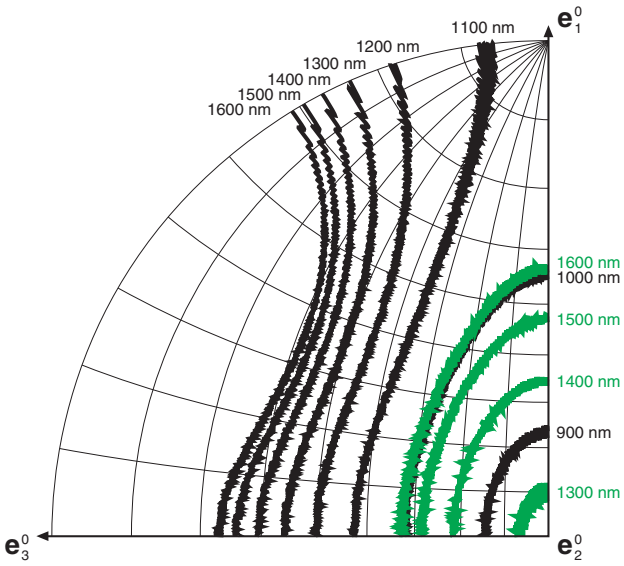

Figure 1 (online color at www.lphys.org) Hobden plot (i.e. stereographic projection of SHG phase matching loci) of $LaBO_2MoO_4$, calculated from refractive index data given in [9]. Black curves indicate type I phase matching (ss-f), green curves indicate type II phase matching (sf-f). The axes $\{\mathbf{e}_i^0\}$ represent the axes of the optical reference system (i.e. the principal axes of the optical indicatrix); they are related to the crystallographic axes $\mathbf{a}$, $\mathbf{b}$, $\mathbf{c}$ as follows: $\mathbf{e}_2^0 \parallel \mathbf{b} \parallel$ twofold axis 2, $\angle(\mathbf{c}, \mathbf{e}_3^0) \approx 35°$, $\mathbf{e}_1^0 = \mathbf{e}_2^0 \times \mathbf{e}_3^0$ (see also [9])

2. Crystallography and crystal growth

Growth of large crystals of $LaBO_2MoO_4$ from the melt has been described in [9], the grown crystals, although being cooled to room temperature very slowly over a period of up to one week, suffer from cracking even at room temperature. The remaining crack-free regions of the crystals, however, are of high optical quality without any stress birefringence and allow the determination of high-quality refractive indices (see [9]) as well as the investigation of SRS properties. Although the refractive indices offer the possibility for phase-matched generation of the second harmonic with type I phase-matching for wavelengths above ≈ 0.89 μm and additionally phase-matching type II for wavelengths above ≈ 1.28 μm of the fundamental wave (see Fig. 1), and the crystal structure is reported to have a pronounced polar symmetry with space group $P2_1$ [13], only a very weak SHG was detected in our previous investigations [9]. From temperature-dependent polarization microscopy no hints to any structural instability could be found in the temperature region between 100 K and 1273 K, especially, no hints to twin formation was found in transmitted polarized light. However, the observation in reflecting light of crystal plates (010) that were polished and etched with hot diluted hydrochloric acid reveals the occurrence of a domain structure of the crystals. An ex-

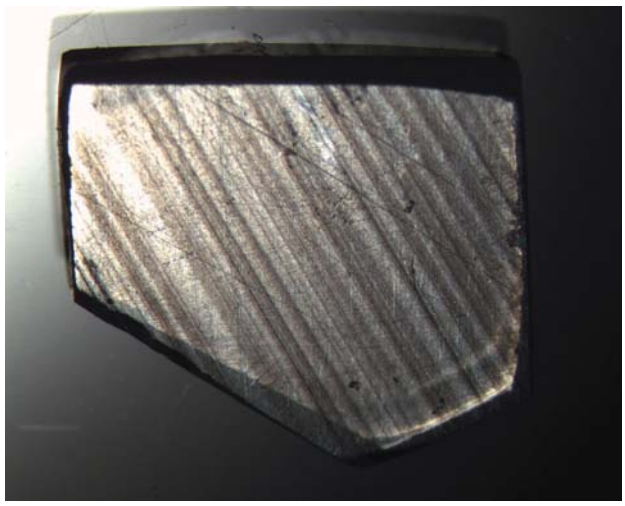

Figure 2 (online color at www.lphys.org) (010) plate of $LaBO_2MoO_4$, polished and etched with hot diluted hydrochloric acid, photographed in reflected light. At room temperature the crystal is a composite of the high- and the low-temperature phases, twin domain walls are visible as parallel lines. The crystal parts of the low-temperature modification show parallel twin boundaries. Note that in transmitted light between crossed polarizers the sample shows perfectly homogeneous extinction and twins are not visible. Width of image 3.1 mm

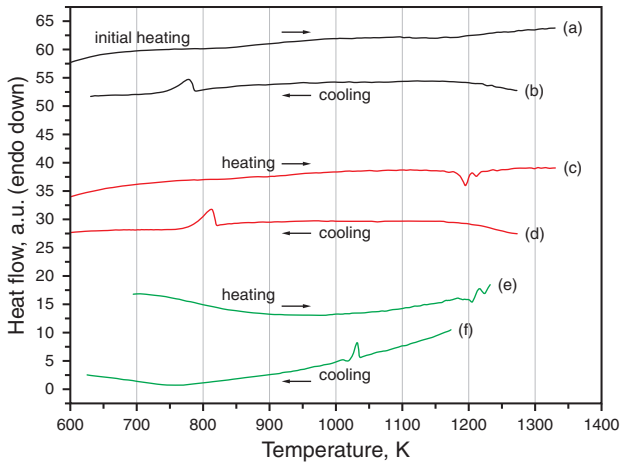

Figure 3 (online color at www.lphys.org) DTA measurements of a crystal of $LaBO_2MoO_4$, using a Perkin Elmer DTA7. Heating rates 20 K/min, dry Argon atmosphere. (a) Initial heating run after sample storage at room temperature for 24 h, $T_{\max} = 1313$ K. (b) Ensuing cooling run. (c) Heating run with $T_{\max} = 1313$ K, following a preceding heating to 1313 K. (d) Ensuing cooling run, dwell time of the sample at temperatures above 1200 K ca. 20 min. (e) Heating run with $T_{\max} = 1213$ K, following a preceding heating to 1213 K. (f) Ensuing cooling run, dwell time of the sample at temperatures above 1200 K ca. 10 min

Characteristic	
Symmetry	monoclinic
Structural phase transition	reversible first order phase transition with large temperature hysteresis; T_{PT} between $\sim$650 K and $\sim$1220 K [a]
Density, g cm^{-3} [13]	$d_{exp.} \approx 5.03$
Melting temperature, K	$T_m \approx 1352$
Method of crystal growth	top-seeding technique
Distribution coefficient k of Nd^{3+}	for $x_{Nd}^{melt} \approx 0.01$: $k_{Nd} \approx 0.54$ for $x_{Nd}^{melt} \approx 0.07$: $k_{Nd} \approx 0.65$
Linear optical character [9]	biaxial negative
Optical transparency range, μm [b] [9]	$\approx$0.33 to $>$3.5
Refractive index (modified Sellmeier equation) of undoped crystal [c] [9]	$n^2(\lambda) = D_1 + \frac{D_2}{(\lambda^2 - D_3)} - D_4\lambda^2$
Phase matching for SHG	type I (ss-f) for $\lambda \geq 0.89$ μm type II (sf-f) for $\lambda \geq 1.28$ μm
Nonlinearity [9]	$\chi^{(2)} + \chi^{(3)}$
Energy of SRS-promoting vibration, cm^{-1} [9]	$\omega_{SRS1} \approx 895$; $\omega_{SRS2} \approx 787$; $\omega_{SRS3} \approx 100$; $\omega_{SRS4} \approx 1690$
Intermanifold branching ratio of luminescence transitions $^4F_{3/2} \rightarrow {}^4I_{9/2-15/2}$, %	$\beta_{J,9/2} \approx 42$; $\beta_{J,11/2} \approx 46$; $\beta_{J,13/2} \approx 11$; $\beta_{J,15/2} \approx 1$
Spectroscopic quality parameter	$X_{Nd} \approx 0.95$
Luminescence decay time	$\tau_{lum}\,(^4F_{3/2}) \approx 115$ μs
SE wavelength, μm	1.0585 and 1.0675 [d]

[a] The measured temperature of the phase transition T_{PT} depends on the thermal history of the sample (see Sec. 2).
[b] For a plate of $\approx$0.5 mm thickness of undoped $LaBO_2MoO_4$. Transmission limit in the visible wavelength range estimated at 50% of maximum transmission.
[c] Sellmeier coefficients: λ is in μm; (ξ^2 is the sum of the squares of the residuals; limit of probable error in parentheses). The angle between the axis $\mathbf{e}_3$ ($= \mathbf{c}/c$) and the principal axis of the optical indicatrix $\mathbf{e}_3^0$ is about 35° in the visible (the same angle is found between $\mathbf{e}_1$ and $\mathbf{e}_1^0$, $\mathbf{e}_2$ is parallel to $\mathbf{e}_2^0$.

	D_1	D_2	D_3	D_4	ξ^2
n_1^0	3.897(2)	0.061(1)	0.039(5)	0.0165(3)	3.0×10^{-8}
n_2^0	3.819(1)	0.0562(9)	0.043(3)	0.0137(2)	1.4×10^{-8}
n_3^0	3,671(1)	0.049(19	0.028(5)	0.0105(3)	2.3×10^{-8}

[d] Due to low sensitivity of the used IR film the SE wavelength of 1.0675 μm could not be recorded by our photographic method.

Table 2 Some physical properties of monoclinic $LaBO_2MoO_4$ and $LaBO_2MoO_4$:Nd^{3+} single crystals (Data at room temperature, unless indicated otherwise)

ample of an etched crystal is shown in Fig. 2. Thermal analysis (DTA, using a Perkin Elmer DTA7) of samples of $LaBO_2MoO_4$ that had been stored at room temperature for several days give a smooth DTA curve with no peaks at the initial heating run. However, in subsequent DTA cooling and heating cycles an exothermal (on cooling) resp. endothermal (on heating) peak that indicates a reversible phase transition, occurs (see Fig. 3). The temperature hysteresis of this phase transformation is rather large and amounts to some hundreds Kelvin, it can be influenced by the dwell time of the sample at temperatures above $\sim$1200 K: for a longer dwell time a larger hysteresis results, see Fig. 3. The dwell time of the sample at room temperature modifies the temperature hysteresis in the same manner, but to a smaller extend. Samples that are stored again at room temperature for several days again do not show a peak in an initial DTA heating run. From this investigation we conclude that $LaBO_2MoO_4$ suffers a first-order structural phase transition that is impeded by slow kinetics and does not proceed completely, neither on heating nor on cooling of the sample. The velocity of the phase transition is substantially controlled by processes of nucleation and crystal growth of both the high-temperature and low-temperature phase, and the amount of remaining (now metastable) phase after the phase transition determines the velocity of the re-transition. Crystals at room temperature usually are a composite of low- and high-temperature phase, see e.g. Fig. 2. The excellent optical homogeneity of the crystals in transmitted polarized light, however, gives no hint to internal stress of the samples, which is a rather unusual feature of a first order phase transition. This signals that there is only very small structural misfit between the high- and low-temperature phase of $LaBO_2MoO_4$. A detailed analysis of the crystal structure of the two modifications of $LaBO_2MoO_4$ is in progress, our preliminary results indicate a symmetry change from point group 2/m at high temperature to the polar point group 2 at room temperature, that is accompanied by twinning. From the de-

Figure 4 (online color at www.lphys.org) Sample of $(La_{1-x}Nd_x)BO_2MoO_4$ with x $\approx$0.047, prepared from a crystal grown from the melt. Size of sample 6.0×5.8×2.4 mm^3

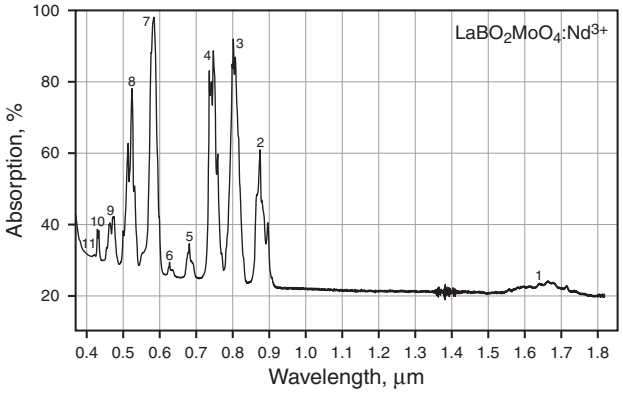

Absorption band-area	Intermanifold transitions $^4I_{9/2} \rightarrow {}^{2S+1}L_{J'}$ [a)]
1	$^4I_{15/2}$
2 *	$^4F_{3/2}$
3 *	$^4F_{5/2}+{}^2H(2)_{9/2}$
4 *	$^4F_{7/2}+{}^4S_{3/2}$
5 *	$^4F_{5/2}$
6 *	$^2H(2)_{11/2}$
7 *	$^4G_{5/2}+{}^2G(1)_{7/2}$
8 *	$^2K_{13/2}+{}^4G_{7/2}+{}^4G_{9/2}$
9	$^2K_{15/2}+{}^2G(1)_{9/2}+{}^2D(1)_{3/2}+{}^4G_{11/2}$
10	$^2P_{1/2}$
11	$^2D_{5/2}$

[a)] Preliminary identification.

Figure 5 Room-temperature orientational absorption spectrum $^4I_{9/2} \rightarrow {}^{2S+1}L_{J'}$ of Nd^{3+} ions in monoclinic $LaBO_2MoO_4$ crystal in the spectral range from 0.4 μm to 1.8 μm wavelength with an identification of its intermanifold transitions. Asterisked band-areas were used as pump absorption bands in SE experiments under filtered Xe-flashlamp radiation

scribed findings so far we can see that in our partly transformed crystals the generation of second harmonic radiation is suppressed by the anti-parallel orientation of the polar axis of the twins; additional fraction of metastable centrosymmetric high-temperature phase does not contribute to SHG at all. In contrast, $\chi^{(3)}$ processes such as SRS are much less affected by this special kind of twinning of the optically very homogeneous samples (see e.g. SRS spectra in [9]).

In $LaBO_2MoO_4$ lanthanum can easily be substituted partially by neodymium. Crystals of $(La_{1-x}Nd_x)BO_2MoO_4$ were synthesized for x up to 0.1 and large single crystals were grown with a mole fraction of neodymium x = 0.010 and x = 0.073 given in the melt. The mole fraction of neodymium of the obtained crystals is x = 0.0054(6) and x = 0.0474(12), respectively, as it was proved by electron beam microprobe analysis. The conditions of crystal growth are similar to those of the growth of undoped $LaBO_2MoO_4$; the phase transition described above for $LaBO_2MoO_4$ is equally found for the Nd^{3+}-doped crystals, including cracking problems with the crystals. However, the optical quality of uncracked parts of the crystals is equally high as of the undoped crystals and allow further optical investigation of the material. In Fig. 4 an example of a sample that was prepared from a grown crystal of $LaBO_2MoO_4$:Nd^{3+} is presented. For our investigation of some spectroscopic properties and stimulated emission of $LaBO_2MoO_4$:Nd^{3+} we used crystal samples with a neodymium portion of $\approx$4.7 mole % (unless indicated otherwise).

3. Spectroscopy and pulsed laser action

The results of our earlier preliminary absorption-luminescence study of the novel $LaBO_2MoO_4$:Nd^{3+} laser crystal [9] allow to determine the energy of the Stark levels of Nd^{3+} lasants related to the pulsed SE in the $^4F_{3/2} \rightarrow {}^4I_{11/2}$ intermanifold of $LaBO_2MoO_4$:Nd^{3+} that was recorded now, together with some corresponding luminescence intensity and kinetic characteristics. These measurements were carried out by traditional methods of absorption and luminescence investigations using high-resolution diffraction spectral devices. In Fig. 5 an orientational overview absorption $^4I_{9/2} \rightarrow {}^{2S+1}L_{J'}$ spectrum of Nd^{3+} activator ions in the monoclinic $LaBO_2MoO_4$:Nd^{3+} crystal, measured at room-temperature (using a (010) plate with C_{Nd} $\approx$4.2 mole %, which corresponds to $\approx 3.7\times10^{20}$ of Nd^{3+} ions per cm^3) is presented. A three-band luminescence $^4F_{3/2} \rightarrow {}^4I_{9/2-13/2}$ spectrum recorded at room temperature with an excitation wavelength of 808 nm is shown in Fig. 6, compared with an analogous spectrum of a $Y_3Al_5O_{12}$:Nd^{3+} crystal with cubic garnet

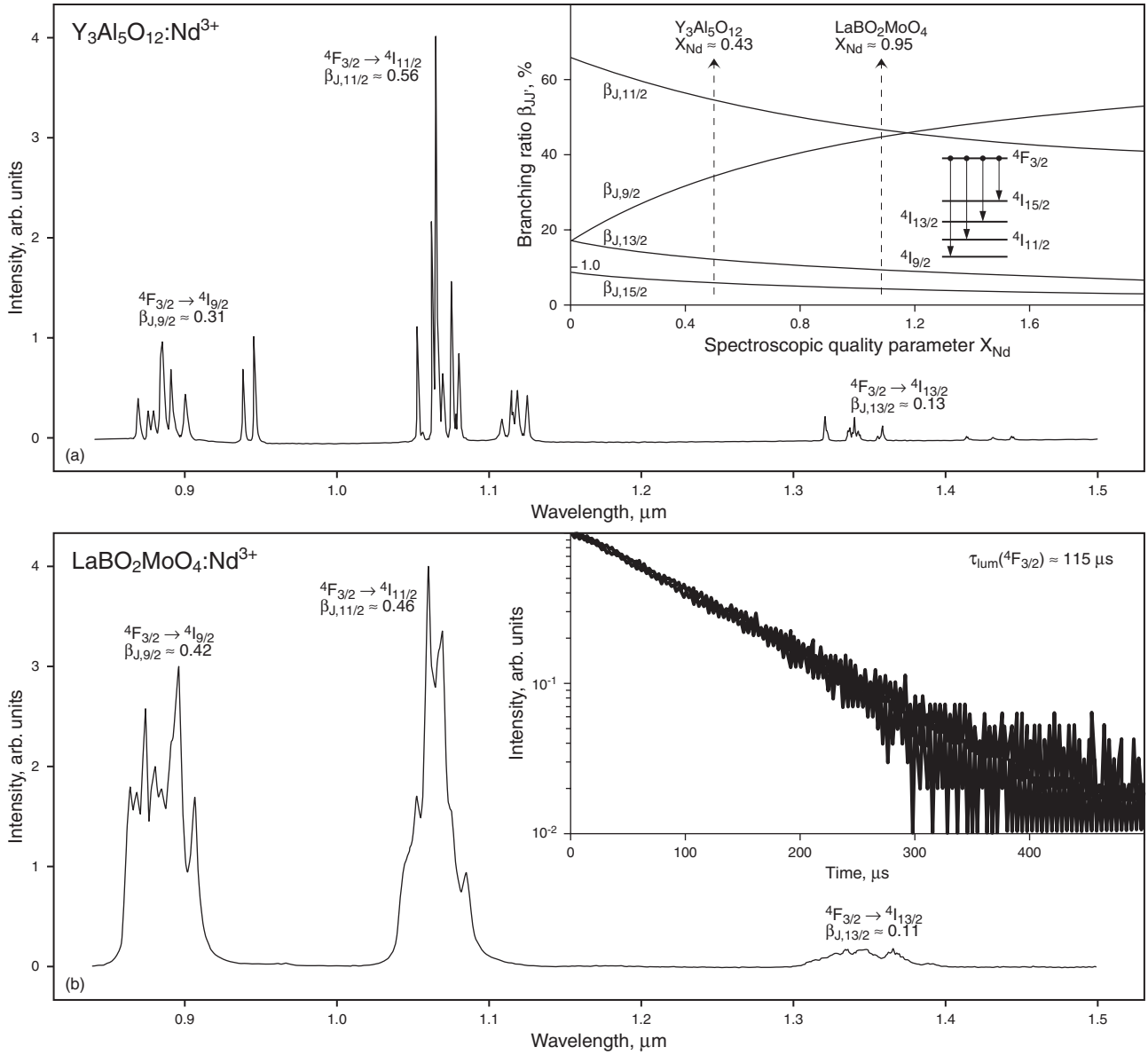

Figure 6 Room-temperature three-band luminescence spectra ${}^4\mathrm{F}_{3/2} \rightarrow {}^4\mathrm{I}_{9/2-13/2}$ of Nd^{3+} activator ions in (a) cubic $Y_3Al_5O_{12}$ and (b) monoclinic $LaBO_2MoO_4$laser crystals with indication of their intermanifold branching ratios $\beta_{JJ'}$. The inset of (a) shows the dependences of $\beta_{JJ'}(X_{Nd})$ [14] and a simplified scheme of ${}^4\mathrm{F}_{3/2} \rightarrow {}^4\mathrm{I}_{9/2-15/2}$ luminescence channels of Nd^{3+} ions. Here, for $\beta_{J,15/2}(X_{Nd})$ the scale was increased ten times and the dashed lines indicate the data of spectroscopic quality parameters for the title crystal and the reference crystal $Y_3Al_5O_{12}$. The inset of (b) shows the single exponential decay time of the metastable (initial laser) ${}^4\mathrm{F}_{3/2}$ state of Nd^{3+} ions in $LaBO_2MoO_4$ crystal

structure (space group $O_h^{10} - Ia\bar{3}d$). An analysis of the luminescence intensity of the Nd^{3+} ions in these two crystals allows to estimate their intermanifold branching ratios

$$\beta_{JJ'} = \frac{A_{JJ'}^{ed}}{\sum\limits_{J'} A_{JJ'}^{ed}},$$

where $A_{JJ'}^{ed}$ is the probability of the electric dipole intermanifold $J \rightarrow J'$ transitions originated from the initial laser ${}^4\mathrm{F}_{3/2}$ state. It should be noted here that the probability of magnetic-dipole transitions from the ${}^4\mathrm{F}_{3/2}$ state is equal to zero [14]. Derived results for $\beta_{JJ'}$ are given in Fig. 6a and Fig. 6b. Using the semi-empirical dependences of $\beta_{JJ'}(X_{Nd})$ [3] in our experimental condition we estimated also (by usual procedure, see, e.g.

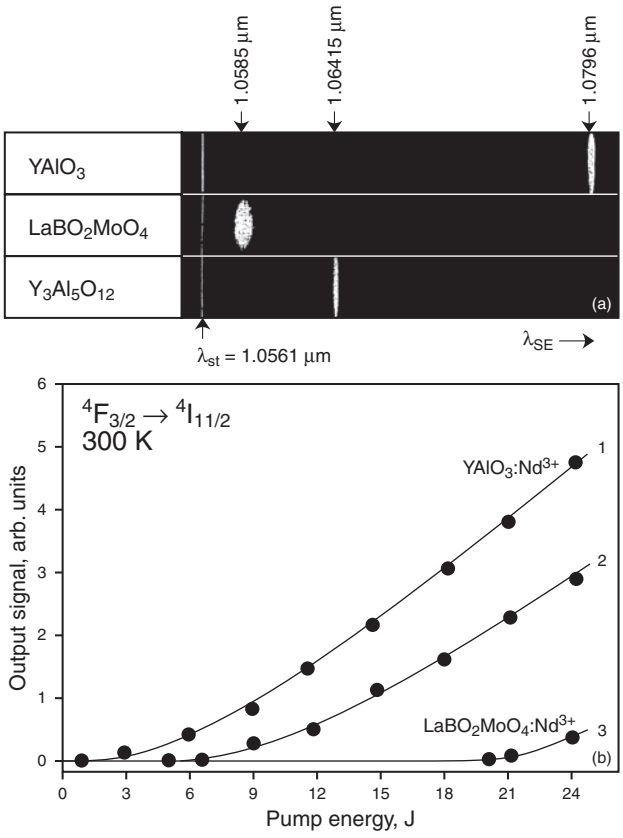

Figure 7 (a) Room-temperature stimulated emission spectra ($^4F_{3/2} \rightarrow {}^4I_{11/2}$ laser channel) of Nd^{3+} ions in monoclinic $LaBO_2MoO_4$ crystal studied (at $\lambda_{SE} = 1.0585$ μm wavelength) and two reference crystals, orthorhombic $YAlO_3$ ($\lambda_{SE} = 1.0796$ μm) and cubic $Y_3Al_5O_{12}$ ($\lambda_{SE} = 1.06414$ μm) recorded under Xe-flashlamp pumping. Wavelength of the standard line $\lambda_{st} = 1.0561$ μm. (b) Output-input dependences for pulsed lasing of an $YAlO_3$:Nd^{3+} crystal at $\lambda_{SE} = 1.0796$ μm wavelength (1), and of $LaBO_2MoO_4$:Nd^{3+} at $\lambda_{SE} = 1.0585$ μm (2) and $\lambda_{SE} = 1.0675$ μm (3). For the latter dependence see text and Fig. 8

[14,15]) the spectroscopic-quality parameters X_{Nd} for our studied crystal $LaBO_2MoO_4$:Nd^{3+} and for the reference garnet crystal $Y_3Al_5O_{12}$:Nd^{3+}. The obtained data are shown in the inset of Fig. 6a. Due to essential differences in the crystal fields of Nd^{3+} in $LaBO_2MoO_4$:Nd^{3+} and in $Y_3Al_5O_{12}$:Nd^{3+} (oxygen coordination, hypersensitive transitions, etc.) the branching ratios of luminescence in channels $^4F_{3/2} \rightarrow {}^4I_{9/2-13/2}$ are quite different between these two kind of laser crystals. The result of measurements of the luminescence decay time of the metastable $^4F_{3/2}$ state of Nd^{3+} ions in $LaBO_2MoO_4$ ($C_{Nd} \approx 4.7$ mole %) is depicted in the inset of Fig. 6b.

The spectroscopic parameters of $LaBO_2MoO_4$:Nd^{3+} that characterise the spectra of Fig. 6b seem to suggest that the crystal field of Nd^{3+}, that substitutes La^{3+} at the

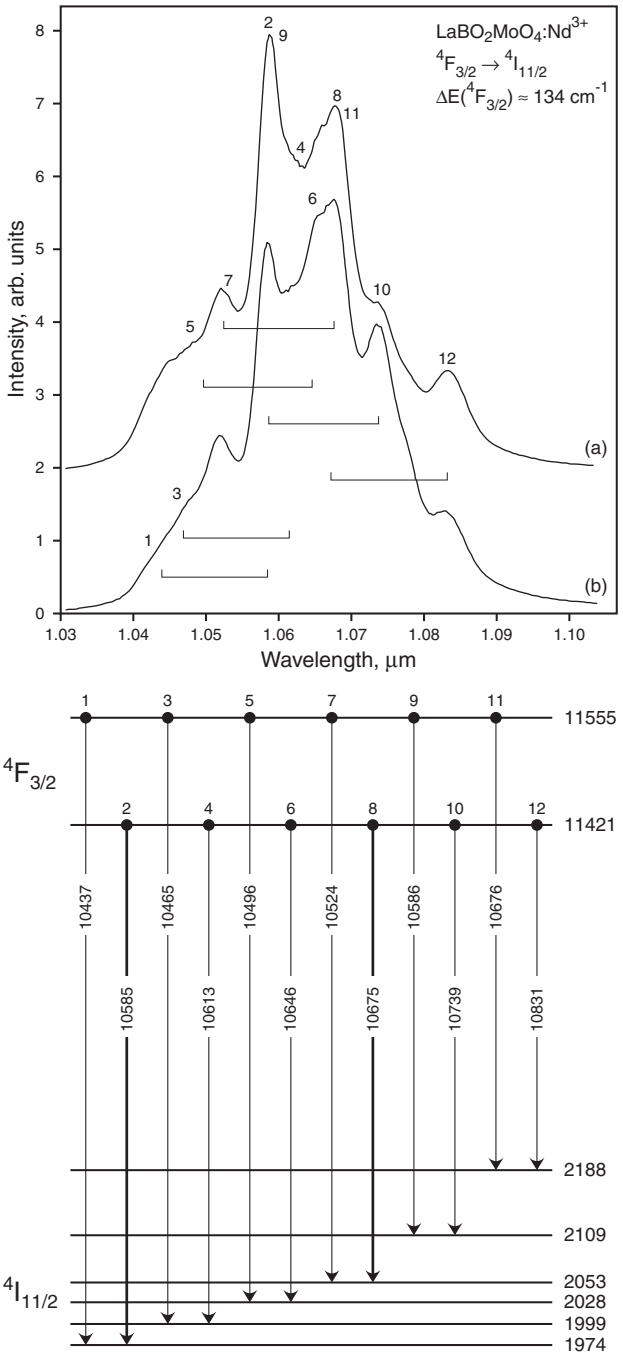

Figure 8 Luminescence spectra $^4F_{3/2} \rightarrow {}^4I_{11/2}$ intermanifold transition for a sample of $LaBO_2MoO_4$:Nd^{3+} with incidence face (100), (spectra (a) and (b) are recorded with different degree of sample rotation around the face normal), and crystal-field splitting scheme of $^4F_{3/2}$ and $^4I_{11/2}$ manifolds (bottom part) of Nd^{3+} ions in our monoclinic $LaBO_2MoO_4$ crystal at room temperature. The energy of the Stark levels is given in cm^{-1} and inter-Stark transition between them in Å. Lines in the spectra and inter-Stark transitions in the scheme are denoted by corresponding numbers to facilitate their comparison. The bold arrows indicate SE transitions. The square brackets in the spectra denote the splitting of the metastable $^4F_{3/2}$ state

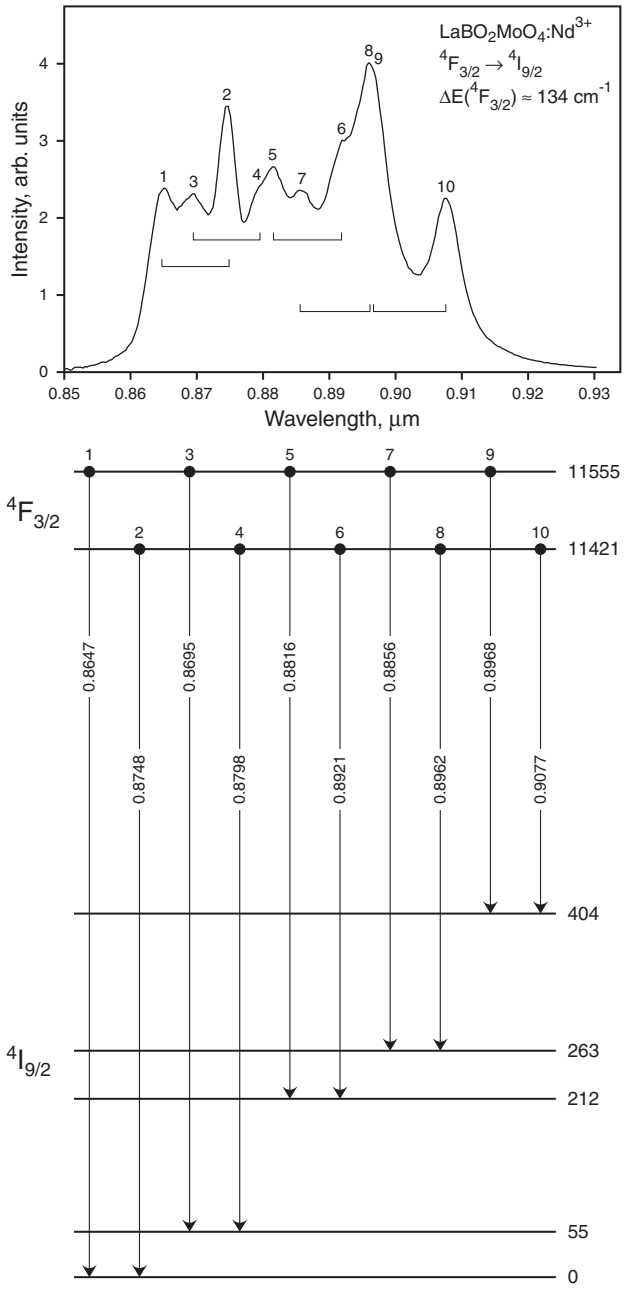

Figure 9 Luminescence spectrum ($^4F_{3/2} \rightarrow {}^4I_{9/2}$ intermanifold transition) and crystal-field splitting scheme of $^4F_{3/2}$ and $^4I_{9/2}$ manifolds (bottom part) of Nd^{3+} ions in our monoclinic $LaBO_2MoO_4$crystal at room temperature. Notations are the same as in Fig. 8

ten-fold coordinated site, could be characterized by slight distortions. Considering that at room temperature crystals of $LaBO_2MoO_4$ mainly represent a composite of a high- and a low-temperature modification with slightly different, but closely related crystal structures (see Sec. 2) a model of disordered crystal field of Nd^{3+} appears to be probable and is in reasonable accordance with the concept of quasi-centre of Nd^{3+} lasants (see, e.g. [3,14,16]. Based on this assumption we can make a rough estimation of the effective cross-section of the luminescence radiation at the SE wavelength by use of the well-known relation of Füchtbauer-Ladenburg for an arbitrary form of the spectrum

$$\sigma^{eff} = \frac{\lambda_{SE}^2 \beta_{J,11/2}}{8\pi\bar{n}^2 \Delta\nu_{lum}^{eff} \tau_{rad}} \approx 10^{-19}\ \mathrm{cm}^{-2}\,.$$

Here we used $\bar{n} \approx 1.95$, which is the average refractive index of the crystal (see [9]), and $\Delta\nu_{lum}^{eff} \approx 140\ \mathrm{cm}^{-1}$, which is the effective width of the $^4F_{3/2} \rightarrow {}^4I_{11/2}$ luminescence band (see Fig. 6b) equal to the ratio of its integral intensity to the peak intensity at $\lambda_{SE} = 1.0585\ \mu$m wavelength. τ_{rad} is the radiative lifetime of the initial state of the luminescence transitions $^4F_{3/2} \rightarrow {}^4I_{9/2-15/2}$, which is equal to $\tau_{lum} \approx 115\ \mu$s (see inset of Fig. 6b).

Laser experiments with a $LaBO_2MoO_4$:Nd^{3+} crystal ($C_{Nd} \approx 4.7$ mole %) at a wavelength of the main generation channel $^4F_{3/2} \rightarrow {}^4I_{11/2}$ of the activator ions were performed under Xe-flashlamp pumping using a confocal optical resonator which was formed by spherical ($r = 500$ mm) dielectric mirrors having high reflectivity ($R \approx 99.5\%$) at the SE wavelength. A crystalline sample without antireflection coating and an ISP-250 type Xe-flashlamp were placed in the focal areas of an elliptical illumination chamber (to avoid UV ageing of the lasing crystal the ISP-250 pumping lamp was surrounded by a tubular ZhS-17 glass filter with transparency above $\approx 0.5\ \mu$m). The spectral composition of the near-IR lasing of the studied crystal was registered by a photographic method (accuracy $\pm 0.0001\ \mu$m) using a high-resolution grating DFS-8 spectrograph and I-1070 type of IR-films. Two Nd^{3+}-ion doped commercial laser crystals, $Y_3Al_5O_{12}$ and $YAlO_3$, with known SE wavelength were measured in our experiments for comparison. The lasing threshold and output SE signals were recorded by commonly used methods with a cooled high sensitivity InSb photo-resistor and appropriate calibrated electronics, as well as a MDR-3 type grating monochromator. Some of the obtained pulsed SE data are shown in Fig. 7. Under the conditions of our laser experiment with the monoclinic $LaBO_2MoO_4$:Nd^{3+} crystal its two-wavelength pulsed SE at 1.0585 μm and 1.0675 μm was recorded. Unfortunately, due to the low sensitivity of the used IR film only strong generation at the shortest wavelength could be recorded photographically.

The recorded room-temperature SE wavelengths were tentatively attributed to corresponding inter-Stark transitions of the Nd^{3+} lasants of the title crystal, despite of our still incomplete knowledge of the structural details at the lasing centres of the crystal. We conducted an analysis of the more intensive luminescence spectra $^4F_{3/2} \rightarrow {}^4I_{9/2}$ and $^4F_{3/2} \rightarrow {}^4I_{11/2}$ of the title crystal (see Fig. 6b), among them the latter acts as the SE channel. The determined Stark levels and identified inter-Stark transitions of the ground $^4I_{9/2}$ and metastable $^4F_{3/2}$ states, as well as

of the terminated $^4I_{11/2}$ laser manifold are presented in Fig. 8 and Fig. 9. As can be seen, room-temperature pulsed SE in our $LaBO_2MoO_4$:Nd^{3+} crystal under Xe-flashlamp pumping occurs at the wavelength of two inter-Stark transitions (11421 cm^{-1} $^4F_{3/2} \rightarrow {}^4I_{11/2}$ 1974 cm^{-1} for $\lambda_{SE} \approx 1.0585$ μm and 11421 cm^{-1} $^4F_{3/2} \rightarrow {}^4I_{11/2}$ 2053 cm^{-1} for $\lambda_{SE} \approx 1.0675$ μm) that originate from the lower level of the metastable $^4F_{3/2}$ state. We believe that the SE potential of the $LaBO_2MoO_4$:Nd^{3+} crystals is not limited only to the recorded pulsed generation in this work. With the availability of pure low-temperature phase crystals of $LaBO_2MoO_4$:Nd^{3+} grown below the structural phase transition, we hope to achieve laser action at additional wavelengths in other practically important generation regimes, including laser action with laser-diode pumping technique.

4. Conclusion

From the results of this investigation it can be concluded that $LaBO_2MoO_4$:Nd^{3+} is a promising material for realization of self-FD and self-SRS lasers. However, at the present stage of our investigations crystals of $LaBO_2MoO_4$:Nd^{3+} are usually (similar to undoped $LaBO_2MoO_4$) a composite of a high- and a twinned low-temperature modification with slight differences in the geometry of the coordination surroundings of the lanthanides, causing disordered crystal field of Nd^{3+} (and probably of further lanthanide dopants such as Pr^{3+}, Er^{3+}, or Yb^{3+}). Therefore, the great challenge on the way towards realization of multifunctional laser properties with $LaBO_2MoO_4$:Nd^{3+} is the growth of untwinned large single crystals of the non-centrosymmetric low-temperature phase, i.e. to master crystal growth at temperatures below the structural phase transition. The title crystals possess simultaneously promising laser properties concerning SE generation (presently Nd^{3+} activator ions) and concerning nonlinear-lasing (SHG and SRS), opening the way to develop multifunctional lasers based on this molybdate borate.

Acknowledgements The authors thank PD Dr. G. Suhr, Institute of Geology and Mineralogy, University of Cologne, for help with electron beam microprobe analysis. Investigations reported here were supported by the Deutsche Forschungsgemeinschaft under sign BE 2147/6-1 and BO 1017/5-1. One of us (A.A.K.) is grateful also to the Russian Foundation for Basic Research and the Russian Academy of Sciences.

References

[1] A.A. Kaminskii, Crystalline Lasers: Physical Processes and Operating Schemes (CRC Press, Boca Raton, 1996); A.A. Kaminskii, Laser Photon. Rev. **1**, 93 (2007).
[2] L.M. Dorozhkin, I.I. Kuratev, N.I. Leonyuk, T.I. Timoshenko, and A.V. Shestakov, Sov. Tech. Phys. Lett. **7**, 555 (1981).
[3] A.A.Kaminskii, in: Photonic Crystals for the Next Century (Int. Workshop Technical Digest, San Sebastian, 2001), p. 32; A.A. Kaminskii, in: B. Di Bartolo and O. Forte (eds.), Frontiers of Optical Spectroscopy. Investigating Extreme Physical Conditions with Advanced Optical Techniques. (Kluwer, Dordrecht, 2005), p. 619.
[4] A.A. Kaminskii, P. Becker, L. Bohatý, K. Ueda, K. Takaichi, J. Hanuza, M. Maczka, H.J. Eichler, and G.M.A. Gad, Opt. Commun. **206**, 179 (2002).
[5] A.A. Kaminskii, P. Becker, L. Bohatý, S.N. Bagaev, H.J. Eichler, K. Ueda, J. Hanuza, H. Rhee, H. Yoneda, K. Takaichi, I. Terashima, and M. Maczka, Laser. Phys. **13**, 1385 (2003).
[6] A.A. Kaminskii, P. Becker, L. Bohatý, H.J. Eichler, A.N. Penin, K. Ueda, J. Hanuza, K. Takaichi, and H. Rhee, Phys. Status Solidi (a) **201**, 2154 (2004).
[7] A.A. Kaminskii, L. Bohatý, P. Becker, J. Liebertz, H.J. Eichler, and H. Rhee, Laser Phys. Lett. **3**, 519 (2006).
[8] A.A. Kaminskii, L. Bohatý, P. Becker, J. Liebertz, L. Bayarjargal, J. Hanuza, H.J. Eichler, H. Rhee, and J. Dong, Laser Phys. Lett. **4**, 660 (2007).
[9] P. Becker, L. Bohatý, H. Rhee, H.J. Eichler, J. Hanuza, and A.A. Kaminskii, Laser Phys. Lett. **5**, 114 (2008).
[10] C. Tu, Z. Zhu, J. Li, Y. Huang, B. Wu, M. Huang, and Z. Chen, Opt. Mater. **27**, 167 (2004).
[11] J.J. Romero, B. Oliveros, L.E. Bausá, Z.D. Luo, and J. García Solé, J. Alloys Compd. **341**, 280 (2002).
[12] A. Brenier, C. Tu, Z. Zhu, J. Li, Y. Wang, Z. You, and B.C. Wu, Appl. Phys. Lett. **84**, 16 (2004).
[13] K.K. Palkina, V.Z. Saifuddinov, V.G. Kuznetsov, B.F. Dzhurinskii, G.V. Lysanova, and E.M. Reznik, Russ. J. Inorg. Chem. **24**, 663 (1979).
[14] A.A. Kaminskii, Laser Crystals, Their Physics and Properties (Springer, Berlin, 1981 and 1990).
[15] A.A. Kaminskii and L. Li, Phys. Status Solidi (a) **26**, 593 (1974).
[16] A.A. Kaminskii, Sov. Phys. JETP **31**, 216 (1970).